Skeletal muscle fasicle engineering is improved by co-culture with myofibroblasts and TGF-β1

Jessica Krieger [Corresp., 1] , **Byungwook Park** [2] , **Christopher R Lambert** [3] , **Christopher Malcuit** [1]

[1] Department of Biomedical Sciences, Kent State University, Kent, OH, United States

[2] Physical Intelligence Department, Max Plank Institute for Intelligent Systems, Stuttgart, Germany

[3] Chemistry & Biochemistry, Worcester Polytechnic Institute, Worcester, Massachusetts, United States

Corresponding Author: Jessica Krieger
Email address: jkrieger@kent.edu

Background. Wound healing in skeletal muscle leads to tissue regeneration or the formation of fibrotic scar tissue and is dependent on the interactions between fibroblasts, myofibroblasts, myogenic cells, and cytokines, such as TGF-β1. Historically, recapitulations of the *in vivo* myogenic tissue regeneration environment utilized simplified *in vitro* models lacking 3D tissue structure and cellular complexity. The objective of this study was to establish a 3D co-culture model of skeletal muscle fascicles through inclusion of multiple cell types normally found in the tissue niche and mimicking wound healing paradigms.

Methods. Three culture systems were compared: cell monolayers grown on 2D dishes and 3D tissues prepared via a self-assembly method or collagen 1-based hydrogel biofabrication. The myogenic impact of TGF-β1 and mono-/co-culture strategies containing human dermal fibroblasts, myofibroblasts, and C2C12 mouse myoblasts was assessed in 2D and 3D environments. qPCR identified gene expression changes during fibroblast to myofibroblast and myoblast differentiation between culture conditions. Changes to cell phenotype and tissue morphology were characterized via immunostaining for myosin heavy chain, procollagen, and α-smooth muscle actin. Tissue elastic moduli were measured with parallel plate compression and atomic force microscopy systems, and a slack test was employed to quantify differences in tissue architecture and integrity.

Results. TGF-β1 treatment improved myogenesis in 3D mono- and co-cultures, but not in 2D. The 3D TGF-β1-treated self-assembled co-culture demonstrated the highest myogenin and collagen 1 gene expression, indicating that the inclusion of myofibroblasts significantly enhanced myogenesis beyond the capacity of fibroblasts or TGF-β1-treatment in monocultures containing only myoblasts. These constructs possessed the greatest tissue stability, integrity, and muscle fiber organization, as demonstrated by their rapid and sustained shortening velocity during slack tests, and the highest Young's modulus of 6.55kPA, approximate half the stiffness of *in situ* muscle. Both self-assembled and hydrogel-based tissues yielded the most multinucleated, elongated, and aligned muscle fiber histology. In contrast, the equivalent 2D co-culture model treated with TGF-β1 completely lacked myotube formation through suppression of myogenin gene expression.

Discussion. These results demonstrate that our 3D co-culture model treated with TGF-β1 more closely mimics myogenesis *in vitro* than 2D or monoculture systems. Tissue engineering can be used to improve *in vitro* models for skeletal muscle development, discovery of therapeutics for muscle regeneration, and research and development of *in vitro* meat products. Critically, this study highlights the impact of TGF-β1 and myofibroblasts as myogenesis accelerators across multiple tissue engineering platforms.

1 # Skeletal muscle fascicle engineering is improved by co-culture with
2 # myofibroblasts and TGF-β1
3
4
5
6

8 Jess Krieger[1], Byungwook Park[2], Christopher R Lambert[3], Christopher Malcuit[1]
9
10
11
12 [1]Department of Biomedical Sciences, Kent State University, Kent, Ohio, USA
13
14 [2]Physical Intelligence Department, Max Plank Institute for Intelligent Systems, Stuttgart,
15 Germany
16
17 [3]Chemistry & Biochemistry, Worcester Polytechnic Institute, Worcester, Massachusetts, USA
18
19
20
21
22
23 Corresponding Author:
24
25
26 Jessica Krieger[1]
27
28
29 Email Address: jkrieger@kent.edu

31
32
33
34
35
36
37
38
39
40
41
42
43
44
45
46

47 **Abstract**

48

49 **Background.** Wound healing in skeletal muscle leads to tissue regeneration or the formation of

50 fibrotic scar tissue and is dependent on the interactions between fibroblasts, myofibroblasts,

51 myogenic cells, and cytokines, such as TGF-β1. Historically, recapitulations of the *in*

52 *vivo* myogenic tissue regeneration environment utilized simplified *in vitro* models lacking 3D

53 tissue structure and cellular complexity. The objective of this study was to establish a 3D co-

54 culture model of skeletal muscle fascicles through inclusion of multiple cell types normally

55 found in the tissue niche and mimicking wound healing paradigms.

56 **Methods.** Three culture systems were compared: cell monolayers grown on 2D dishes and 3D

57 tissues prepared via a self-assembly method or collagen 1-based hydrogel biofabrication. The

58 myogenic impact of TGF-β1 and mono-/co-culture strategies containing human dermal

59 fibroblasts, myofibroblasts, and C2C12 mouse myoblasts was assessed in 2D and 3D

60 environments. qPCR identified gene expression changes during fibroblast to myofibroblast and

61 myoblast differentiation between culture conditions. Changes to cell phenotype and tissue

62 morphology were characterized via immunostaining for myosin heavy chain, procollagen, and α-

63 smooth muscle actin. Tissue elastic moduli were measured with parallel plate compression and

64 atomic force microscopy systems, and a slack test was employed to quantify differences in tissue

65 architecture and integrity.

66 **Results.** TGF-β1 treatment improved myogenesis in 3D mono- and co-cultures, but not in 2D.

67 The 3D TGF-β1-treated self-assembled co-culture demonstrated the highest myogenin and

68 collagen 1 gene expression, indicating that the inclusion of myofibroblasts significantly

69 enhanced myogenesis beyond the capacity of fibroblasts or TGF-β1-treatment in monocultures

70 containing only myoblasts. These constructs possessed the greatest tissue stability, integrity, and

71 muscle fiber organization, as demonstrated by their rapid and sustained shortening velocity

72 during slack tests, and the highest Young's modulus of 6.55kPA, approximate half the stiffness

73 of *in situ* muscle. Both self-assembled and hydrogel-based tissues yielded the most

74 multinucleated, elongated, and aligned muscle fiber histology. In contrast, the equivalent 2D co-

75 culture model treated with TGF-β1 completely lacked myotube formation through suppression of

76 myogenin gene expression.

77   **Discussion.** These results demonstrate that our 3D co-culture model treated with TGF-β1 more

78   closely mimics myogenesis *in vitro* than 2D or monoculture systems. Tissue engineering can be

79   used to improve *in vitro* models for skeletal muscle development, discovery of therapeutics for

80   muscle regeneration, and research and development of *in vitro* meat products. Critically, this

81   study highlights the impact of TGF-β1 and myofibroblasts as myogenesis accelerators across

82   multiple tissue engineering platforms.

83

84   **Introduction**

85

86   Muscle regeneration occurs when muscle fibers are damaged during exercise or injury and

87   quiescent satellite cells are activated to a proliferative myoblast phenotype (Hill, Wernig, &

88   Goldspink, 2003). They differentiate as they begin expressing the myogenic transcription factor

89   myogenin (MYOG) and terminally exit the cell cycle. Their fusion with an injured muscle fiber

90   or other myoblasts forms a nascent syncytial myofiber (Charge & Rudnicki, 2004; Le Grand &

91   Rudnicki, 2007). Fibroblasts support and stabilize muscle fiber architecture and biomechanics

92   through basement membrane synthesis and facilitate muscle regeneration with extracellular

93   matrix (ECM) deposition and remodeling (Murphy, Lawson, Mathew, Hutcheson, & Kardon,

94   2011; Sandbo & Dulin, 2011; Sanes, 2003). The interaction between myoblasts and fibroblasts,

95   two predominant cell types involved in skeletal muscle regeneration, with surrounding ECM and

96   trophic factors determine healing outcomes. TGF-β1, produced by multiple cell types during

97   wound healing, is a primary mediator of the mechanical, biochemical, and cellular behaviors

98   observed in the response of muscle to injury (Karalaki, Fili, Philippou, & Koutsilieris, 2009).

99   TGF-β1 signaling differentiates fibroblasts into myofibroblasts, which are important producers

100   of collagen I (COL I), the main protein component of scar tissue, and α-smooth muscle actin (α-

101   SMA), a highly contractile form of actin (Mendias et al., 2012). Normally these proteins are

102   transiently expressed during muscle regeneration and contribute to tissue remodeling by

103   temporarily providing physical substrates and biochemical cues for muscle fiber regeneration,

104   but excessive TGF-β1-mediated myofibroblast activation leads to ECM accumulation and tissue

105   stiffening that decreases the ability of myoblasts to regenerate muscle (Gilbert et al., 2010;

106   Smith, Lee, Ward, Chambers, & Lieber, 2011).

107

108 The use of culture models consisting solely of myoblasts to investigate skeletal muscle
109 regeneration is narrow in scope and validity and prevents effective screening of therapeutics.
110 Using co-culture systems allows the bi-directional signaling between fibroblasts and myoblasts
111 that attenuates and stabilizes myogenesis. Additionally, while 2D *in vitro* cell culture systems
112 have demonstrable value, they are limited by a number of factors that have unwanted influence
113 on cell behavior. After isolation, primary cells quickly lose their *in situ* characteristics in
114 response to a mechanically and biochemically alien environment (Janson, Rietveld, Willemze, &
115 El Ghalbzouri, 2013). Fibroblasts and muscle stems cells are particularly sensitive to mechanical
116 stimulation, and the rigidity of substrata can mask the cellular responses under investigation
117 (Engler, Sen, Sweeney, & Discher, 2006; Godbout et al., 2013). It is therefore highly valuable to
118 further optimize the *in vitro* recapitulation of the *in vivo* environment. In this regard, myogenesis
119 should be studied within the context of tissues rather than cell culture plates. Engineered tissue
120 that contains aligned muscle fibers embedded within connective tissue is biomimetic to muscle
121 fascicles observed *in vivo* (Turrina, Martinez-Gonzalez, & Stecco, 2013) and is therefore our
122 design target for modeling skeletal muscle.

123

124 Signaling of profibrotic factors such as TGF-β1 can deregulate the regenerative capacity of
125 muscle and drive fibrosis when in excess (Lieber & Ward, 2013; Mann et al., 2011) but regularly
126 contribute to muscle regeneration at moderate levels. The use of TGF-β1 may therefore be a
127 means to organize tissue-engineered skeletal muscle development *in vitro*. In this study, we have
128 utilized TGF-β1 supplementation in 3D self-assembled, scaffoldless tissue constructs (Gwyther
129 et al., 2011) and collagen 1-based hydrogels consisting of monocultures of mouse myoblasts,
130 human fibroblasts, or TGF-β1-differentiated myofibroblasts, and their combination in co-culture.
131 We found that TGF-β1 signaling in 3D improves myogenesis in myoblast monocultures, and the
132 presence of myofibroblasts further enhances this effect. Our scaffoldless self-assembled tissues
133 and hydrogels both similarly possessed enhanced myogenesis, indicating this technique has wide
134 applicability across a variety of skeletal muscle tissue engineering platforms. However, 2D
135 experiments demonstrated an inhibition of myogenesis in both mono- and co-culture conditions.
136 Our data suggest that 2D *in vitro* models of skeletal muscle are insufficient to provide a complete
137 understanding of the idiosyncratic mechanisms of skeletal muscle regeneration. This information

138   underscores the necessity for replicating the *in vivo* environment *in vitro* by using tissue

139   engineered culture models.

140

141   **Materials and Methods**

142

143   **Cell and tissue culture**

144   Cultures consisting solely of human neo-natal dermal fibroblasts (passage 4 hDFs, PCS-201-010,

145   ATCC, Manassas, VA) or mouse myoblasts (pre-passage 4 C2C12s, CRL-1772, ATCC) were

146   plated on standard cell culture plates at 1 k/cm² in growth media (GM) consisting of DMEM

147   (Gibco, Waltham, MA), 10% fetal bovine serum (FBS, Hyclone, Pittsburg, PA), 1%

148   penicillin/streptomycin (P/S, Gibco). To promote differentiation of fibroblasts to myofibroblasts,

149   some fibroblasts were incubated with 1 ng/mL TGF-β1 (Peprotech, Rocky Hill, NJ) for 6 days

150   between P4 and P5. C2C12s and P4 fibroblasts and myofibroblasts were trypsinized,

151   resuspended in GM, and seeded at a 1:1 ratio either on standard cell culture plates at 20 k/cm² or

152   in 3D self-assembled tissue constructs. To develop 3D self-assembled tissues, cell suspensions

153   were added into custom 2% agarose ring molds with a central post at 350K cells per millimeter

154   of post diameter (Fig 1). Hydrogels were produced from a protocol adapted from Baaijens et. al

155   [18] where 1.5×10^6 C2C12s alone or a 1:3 ratio of fibroblasts/myofibroblasts and C2C12s were

156   resuspended in 42% GM, 54% rat collagen type 1 (3mg/mL, Corning Life Sciences), and 2.7%

157   NaOH (0.5M). The hydrogel mixture was poured between house-shaped Velcro anchors super

158   glued to the bottom of a six well plate and gelled for 45 minutes before adding GM. After 24

159   hours, media were switched to differentiation medium (DM) composed of DMEM, 2% horse

160   serum (Sigma-Aldrich, St. Louis, MO), and 1% P/S, with or without 1 ng/mL TGF-β1. Media

161   was changed every 2-3 days for 7 days, after which cells and tissues underwent qPCR, ICC or

162   IHC, or mechanical characterization. See Figure 1 for listing of experimental groups.

163

164   **Gene expression analysis**

165   Total RNA was isolated from cultures using TriZol reagent (Life Technologies, Carlsbad, CA)

166   according to the manufacturers recommended instructions. cDNA was reverse transcribed from

167   1 μg total RNA using qScript SuperMix (Quanta Biosciences, Gaithersburg, MD) according to

168   manufacturers instructions. qPCR was carried out using a 5 ng equivalent of cDNA in a 1X

169 reaction of PerfeCTa SYBR Green SuperMix (Quanta Biosciences) and 250 nM each (forward

170 and reverse) custom oligonucleotide primers (Integrated DNA Technologies, Coralville, IA)

171 generated by using PrimerBlast (National Center for Biotechnology Information, Bethesda, MD).

172 Reactions were carried out on an Eppendorf RealPlex2 qPCR system, and fold changes in gene

173 expression were calculated using the ΔΔCT method using species-specific GAPDH primers.

174 Primer sequences are listed in S1 Table. Human collagen 1 and α-SMA expression levels in the

175 2D FibCon condition were used as the reference group for fibroblast gene expression, and mouse

176 myogenin gene expression levels of 2D MyoCon were used as a reference for myoblasts. N = 5

177 for all groups.

178

179 **Immunostaining**

180 2D and 3D cultures were assessed qualitatively with immunostaining. 2D cultures were fixed

181 with 4% formaldehyde for 20 minutes, and 3D cultures were fixed for 2 hours. 3D self-

182 assembled tissues were then submerged in OCT media, frozen for cryosectioning, sectioned at

183 30μm thick, and applied to glass slides. Hydrogels remained unsectioned for whole-mount

184 imaging. After fixing, 2D and 3D samples were permeabilized with 0.1% Triton X-100 in PBS

185 for 20 minutes, and then incubated with a blocking solution consisting of 5% FBS in PBS for 20

186 minutes. Following blocking, samples containing myoblasts were stained with rhodamine

187 phalloidin (R415, 1:40 dilution, Life Technologies) and/or myosin heavy chain (MF-20, 1:50,

188 Developmental Studies Hybridoma Bank, Iowa City, IA), procollagen (M-38, 1:50,

189 Developmental Studies Hybridoma Bank) or α–SMA (A 2547, 1:1000, Sigma-Aldrich) primary

190 antibodies. Primary antibody staining was followed by incubation with Alexa-Fluor 488 or 564

191 secondaries (1:250, Life Technologies) and DAPI (1:50,000, Invitrogen, Carlsbad, CA). Imaging

192 of 2D samples was completed with an Olympus IX81 microscope (Olympus corporation of the

193 Americas, Center Valley, PA), 3D self-assembled tissues were imaged with an Olympus

194 Fluoview FV1000 Confocal Microscope, and hydrogels were imaged with an Olympus Fluoview

195 FV1000MPE multiphoton microscope. All images were processed with ImageJ (Version 1.48,

196 National Institute of Health, Bethesda, MD). The total area of procollagen staining was measured

197 in 2D FibCon and FibTGFβ images and divided by the total number of nuclei to find the average

198 area of procollagen staining per cell. Increased area procollagen signal was extrapolated as a

199 change of in cell shape and increased cell spreading. Circularity of DAPI stained fibroblast

200   nuclei was measured to compare changes in cyto- and nucleoskeletal shape. N = 13 images for

201   each group. 2D MyoCon and CoCon images were also processed to measure changes in myotube

202   alignment. In each image, the myotubes formed angles with a common axes (x or y). The

203   standard deviations of the angles from each image were measured to compare the variation in

204   each group, with smaller averaged standard deviations for one sample image indicating higher

205   myotube alignment. N = 8-9 images for each sample.

206

207   **Slack Test**

208   The slack test method has been adapted by our lab to indirectly measure and compare tissue

209   integrity, ECM maturity, and muscle fiber development between engineered samples. Self-

210   assembled tissue constructs were released from tension in culture and their shortening lengths

211   were recorded over time. The initial lengths (μm, L_i) of rings were recorded across their longest

212   axis while they remained on their posts. Rings were then removed from the agarose posts,

213   suspended in PBS (37°C) on a submerged horizontal microbeam from the Microsquisher system

214   (CellScale, Ontario, Canada), and points across their longest axis were tracked to measure

215   shortening every 3 minutes for 27 minutes. The final length (L_f) was divided by the initial length

216   and multiplied by 100 to determine the percent shortening. Tissues were then stored in their

217   respective medias for 24 hours at 37°C and imaged with a stereoscope. ImageJ was used to

218   calculate the inner circumferential area (C_1) and outer circumferential area (C_2) of each ring. C_1

219   was divided by C_2 and multiplied by 100 to yield the percent of tissue area shrinking in CoCon

220   and CoTGFβ samples.

221

222   **Tissue elastic moduli assessments**

223   For calculations of the elastic stiffness of self-assembled engineered tissues, two methods of

224   mechanical characterization were used: a compression-based system to generate slopes from

225   stress-strain curves and atomic force microscopy (AFM). Tissue constructs were sectioned into

226   4-5 pieces with diameters between 250-500 μm and were compressed in a PBS fluid bath (pH

227   7.4, 37°C) using a Microsquisher (Cellscale). Tissues were compressed to 40% of their original

228   diameter at a rate of 1% per second using microbeams with diameters between 0.2-0.3048 mm.

229   Force-displacement curves were generated and the slope of the linear portion of the curve was

230   extrapolated as the elastic modulus of the tissue. Slopes were averaged for each 3D condition

231   with N = 8-12 section samples per group.

232

233   Tissue elastic moduli were measured by an Asylum MFP3D-Bio AFM (Asylum Research, Santa

234   Barbara, CA) through a nano-indention method using MFP-3D software (Version 13.04.77).

235   Force-distance curves were determined using equations 1 and 2:

236   $\quad$ 1) $F(\delta) = \frac{4\sqrt{R}}{3} \frac{E}{1-\nu^2} \delta^{3/2}$

237   $\quad$ 2) $F(\delta) = \frac{E}{1-\nu^2} \frac{2\tan\alpha}{\pi} \delta^2$

238

239   Where F is the measured force, E is the local Young's modulus, R is the cantilever's tip radius

240   (for a spherical tip), α is the cantilever's tip angle (for a cone tip), ν is the Poisson's ratio of the

241   sample (assumed as 0.5 for an incompressible material), and δ is the sample indentation.

242   Pyramidal tips with a nominal tip radius 20 nm, 200 µm in length, 20 µm in width, and a tip

243   semi-angle of 15° on silicon nitride triangular V-shaped cantilevers with a nominal spring

244   constant of 0.06 N/m (DNP-10; Bruker Inc., Camarillo, CA) were employed. The recorded force-

245   distance curves were analyzed in MATLAB and statistical analysis was done using SPSS (Ver.

246   17.0, IBM, Somers, NY).

247

248   **Statistics**

249   Statistical analyses were performed with two-tailed unpaired t-tests and one-way ANOVAs using

250   GraphPad Prism (Version 4, GraphPad Software) and statistical significance was defined as p <

251   0.05. Means are reported with standard error bars in bar graphs. Skew coefficients were

252   calculated in Excel (Version 14.6.4, Microsoft).

253

254   **Results**

255

256   **Fibroblast to myofibroblast differentiation is observed in 2D cultures treated with TGF-β1,**

257   **regardless of myoblast presence.**

258   2D fibroblast-only cultures displayed increased α-SMA staining in TGF-β1-treated samples (Fig

259   2A, B) and increased α-SMA gene expression (p < 0.01, Fig 3A), indicating their differentiation

260   to myofibroblasts. There was no significant difference in collagen 1 transcription between any

261 2D conditions containing fibroblasts or myofibroblasts (Fig 3B), but post-translational control of
262 the protein differed with TGF-β1 treatment. Fibroblasts in the control group were spindle-shaped
263 and displayed smaller areas of procollagen signal per cell nuclei (Fig 2C, I), while TGF-β1
264 treatment significantly increased the area of procollagen staining per nuclei by 32.2 % (p <
265 0.0001, Fig 2D, I) and enhanced the secretion of procollagen out of the cell (red arrow in 2D).
266 Nuclei circularity was also increased in 2D FibTGFβ samples (p < 0.0001, Fig 2J), indicating a
267 widening of the nucleoskeleton accompanying increased cell spreading, compared to the more
268 elongated nuclear shape in control conditions. Enhanced cell proliferation was also observed
269 with TGF-β1 treatment (p < 0.0001, Fig 2K), as recorded by average number of nuclei per field
270 of view. α-SMA gene expression in 2D CoCon samples was similar to transcript levels of the
271 fibroblast-only control group, but was significantly upregulated in 2D CoTGFβ conditions (p <
272 0.01, Fig 3A).

273

274 **Myogenesis is suppressed in 2D cultures with TGF-β1 supplementation and in the presence**
275 **of fibroblasts, yet fibroblasts increase myotube alignment.**
276 Robust myotube formation was present in 2D MyoCon samples (Fig 2E), decreased with
277 exposure to TGF-β1 (Fig 2F) or in co-culture with fibroblasts (Fig 2G), and completely inhibited
278 in myofibroblast co-cultures supplemented with TGF-β1 (Fig 2H). MYOG gene expression in
279 the 2D MyoTGFβ and 2D CoCon conditions were similar to each other and both displayed
280 significant MYOG downregulation in comparison to 2D MyoCon. 2D co-cultures exposed to
281 TGF-β1 showed the lowest MYOG expression of any group (p < 0.01, Fig 3C). Notably, despite
282 diminishing myogenesis, fibroblasts organized myotube formation by increasing their alignment
283 in 2D CoCon samples (p < 0.001, Fig 2L).

284

285 **In comparison to fibroblasts grown on plastic, self-assembled tissues containing only**
286 **fibroblasts have a suppressed ability to assume a myofibroblast phenotype.**
287 In comparison to 2D fibroblast-only controls, expression of procollagen was dramatically
288 downregulated in fibroblast-only tissues, and this was not improved by TGF-β1 exposure (p <
289 0.01, Fig 3B). α-SMA staining was absent in 3D FibCon samples (S1 Fig, A), but was somewhat
290 increased with TGF-β1 treatment (S1 Fig, C). 3D FibCon and FibTGFβ α-SMA gene expression
291 was transcriptionally downregulated to an even greater degree than procollagen, yet these values

292   were not significantly different from each other (p < 0.01, Fig 3A). Fibroblast/myofibroblast-
293   only tissues were quite fragile; they would easily rupture during handling (arrow, Fig 4D) and
294   would sometimes collapse, losing their annular shape (Fig 4C, F). Despite their fragility, their
295   surfaces were smooth and homogenous (Fig 4S). Interestingly, the average thickness of
296   constructs containing myofibroblasts treated with TGF-β1 was 33.2 % larger than respective
297   controls (p < 0.01, Fig. 5F), similar to the myofibroblast hypertrophy seen in 2D FibTGFβ.
298
299   **TGF-β1 supplementation improves myoblast differentiation and alignment in myoblast-**
300   **only self-assembled tissues.**
301   3D myoblast-only groups differed in their degree of myogenesis and their myotube formation
302   patterns. 3D MyoCon contained myotubes that had some degree of organization but generally
303   weren't aligned (Fig 6A, B), whereas myoblast samples treated with TGF-β1 had myotubes that
304   were aligned along their circumferential axis (white filled arrow, Fig 6E, F). Gene expression
305   profiles indicated that 3D MyoCon samples had significantly lower myogenin expression than
306   both the 2D MyoCon control and 3D MyoTGFβ condition (p < 0.01, Fig 3C), but the 2D control
307   and 3D TGFβ treated condition were not significantly different from each other. α-SMA was
308   present in both untreated (Fig 6C, D) and TGF-β1 treated (Fig 6G, H) myoblast constructs, but
309   quantitative differences were not assessed. Observable in the α-SMA stained sections are fissures
310   and breaks in the tissue (white asterisks, Fig 6C, G). Additionally, the surfaces of myoblast-only
311   tissues presented nodular syncytium of fused myoblasts lacking the anchorage necessary to
312   elongate and form myotubes (arrow, Fig 6I-K), and this was macroscopically observable
313   (unfilled arrows, Fig 4T). Heterogeneous tissue patterning is also seen here, with many ripples
314   along the tissue surface, large budges (filled arrow, Fig 4T), and regions of varying density.
315
316   **In self-assembled co-cultures, fibroblasts and myofibroblasts homogenize tissue surfaces,**
317   **myofibroblasts improve myotube formation, and TGF-β1 enhances myogenesis.**
318   Addition of fibroblasts or myofibroblasts smoothened the surface of co-culture tissues (Fig 4U),
319   similarly to fibroblast- or myofibroblast-only samples, and these constructs lacked the studding
320   of nodular syncytium seen in myoblast-only tissues. Co-culture conditions (Fig 4M, P) appeared
321   visually denser than their fibroblast- (Fig 4A, D) and myoblast-only (Fig 4G, J) counterparts.
322   Similar to the hypertrophy observed in 2D and 3D myofibroblast conditions treated with TGF-

323 β1, CoTGFβ tissues were 27.9 % thicker than CoCon (p < 0.01, Fig 5F). While human
324 fibroblast/myofibroblast α-SMA gene expression was decreased in all 3D conditions compared
325 to the 2D FibCon group, it was significantly higher in 3D CoCon and CoTGFβ compared to 3D
326 fibroblast-only tissues (p < 0.01, Fig 3A), and co-culture transcription levels were not influenced
327 by TGF-β1 supplementation. A non-species specific α-SMA antibody was visible within
328 myotubes, where CoCon samples showed α-SMA within punctate and short myotubes (Fig 7A),
329 while those in CoTGFβ tissues were elongated and more mature (Fig 7C), indicating that TGF-
330 β1 facilitated the development of bundles of myotubes aligned in parallel. Additionally, collagen
331 1 expression was increased in 3D co-cultures compared to 3D fibroblast/myofibroblast-only
332 cultures (p < 0.01, Fig 3B), but CoCon constructs were not significantly different from the 2D
333 FibCon condition. Interestingly, collagen 1 gene expression was highest in 3D CoTGFβ samples,
334 which was also the condition of highest MYOG expression (p < 0.01).

335

336 3D CoCon constructs containing fibroblasts frequently presented dense bulges with thickened
337 regions of cells composed of differentiating myoblasts (Fig 7E, F) between thinner regions
338 absent of MyHC staining (Fig 7H, I); this heterogeneous tissue architecture can also be seen
339 macroscopically (arrow, Fig 4M). CoCon constructs contained myotubes that were short but
340 numerous. Some myotubes fused from one wall of the tissue to another, so that during
341 sectioning, cross sections of myotubes are apparent (filled arrows, Fig 7E, F). In contrast,
342 CoTGFβ samples containing myofibroblasts had myotubes that were thicker and more
343 multinucleated (Fig 7G, J, K). These tissues also had many cross-sections of myotubes (filled
344 arrow, Fig 7J), but additionally contained much longer circumferentially aligned myotubes than
345 in control co-culture samples (unfilled arrow, Fig 7G). MYOG expression in 3D CoTGFβ
346 constructs was significantly higher than all other groups (p < 0.01, Fig 3C), while MYOG
347 expression in 3D CoCon constructs was suppressed compared to 2D MyoCon (p < 0.01), and
348 was not significantly different from 3D MyoCon. This data demonstrates that addition of
349 fibroblasts with myoblasts in 3D co-culture does not improve myogenesis beyond what is
350 observed in cultures consisting solely of myoblasts, and TGF-β1 supplementation is a
351 myogenesis-promoting factor.

352

353 **Zero-force velocity is greatest in co-culture with TGF-β1 supplementation in slack tests**

354   Slack tests are a measurement of zero force velocity tissue shortening resulting from the recoil of
355   stretched elastic elements and myofibrillar filament sliding in sarcomeres. Slack tests assess
356   acto-myosin kinetics that are independent of Ca^{2+} activation, which provides biomechanical
357   information about extracellular matrix networking, MHC isoform and muscle fiber type, and
358   muscle organ characteristics (Claflin & Faulkner, 1985; Josephson & Edman, 1998; Reggiani,
359   2007). The initial maximum lengths of self-assembled tissue constructs were recorded prior to
360   removal from their posts (white arrow, Fig 5A). Constructs were then released from tension and
361   their lengths measured every 3 minutes (Fig 4A, D, G, J, M, P) for 27 minutes (Fig 4B, E, H, K,
362   N, Q) and allowed to slack over 24 hours (Fig 4C, F, I, L, O, R). These time points were selected
363   because shortening was no longer visibly distinguishable after 25 minutes of the assay, but
364   continued at a slowed rate over 24 hours. While all groups shortened significantly from their
365   original size ($p < 0.001$, Fig 5B), tissues containing only fibroblasts or myofibroblasts shortened
366   the least, with 3D FibCon remaining 87.3% and FibTGFβ 85.4% their original size.
367   Fibroblast/myofibroblast tissues were the only cell-content matched tissue group that did not
368   display significantly different final length values from each other. Myoblast tissues underwent
369   significantly greater shortening than fibroblast/myofibroblast samples: MyoCon rings shrank to
370   69.4% and MyoTGFβ to 62.2% their initial diameter. Co-culture tissues underwent the greatest
371   alteration, however. CoCon underwent the most significant shortening compared to all other
372   groups (48.7%), and CoTGFβ was the second most shortened group (55.1%). Plotting tissue
373   length changes over time shows most of the length change occurs within the first 3 minutes and
374   slows considerably by 15 minutes (Fig 5C), with co-culture samples displaying the highest
375   velocities. Interestingly, after 24 hours, CoTGFβ tissues (Fig 4R) showed an even greater degree
376   of sample shortening than CoCon (Fig 4O). Since reference points for tracking changes in length
377   were not conserved overnight, their inner circumferential areas (C_1) were divided by their
378   respective outer circumferential areas (C_2, Fig 5A) to yield percent differences in contraction
379   between co-culture groups. CoCon constructs had significantly larger inner cross sectional areas
380   than the CoTGFβ conditions, indicating a greater degree of tissue shrinkage in TGF-β1 treated
381   co-culture rings ($p < 0.05$, Fig 5E). In summary, while TGF-β1 exposure for fibroblast-only
382   samples did not lead to significantly more zero-force shortening in comparison to untreated
383   controls, TGF-β1 positively impacted shortening of myotubes within myoblast-containing

384 tissues, and the interactions between TGF-β1-treated myofibroblasts and myoblasts promoted the
385 greatest degree of shortening.

386

387 **Tissue elastic moduli increase in co-culture and with TGF-β1 exposure.**

388 Using the parallel plate compression system, the Young's modulus for sectioned self-assembled
389 tissues was determined to be 2.04 kPa for FibCon, 0.81 kPa for FibTGFβ, 3.32 kPa for MyoCon,
390 3.86 kPa for MyoTGFβ, 4.47 kPa for CoCon, and 6.55 kPa for CoTGFβ (Fig 5H). FibCon and
391 FibTGFβ tissues were significantly softer than CoCon and CoTGFβ (p < 0.001). While MyoCon
392 and MyoTGFβ were also significantly softer than CoTGFβ (p < 0.001), TGF-β1 did not
393 significantly increase stiffness of samples containing only myoblasts. Similarly, while TGF-β1
394 treatment increased the stiffness of CoTGFβ, it was not a significant increase with respect to
395 CoCon. Consequently, AFM was used to increase the sensitivity of measurements of elasticity at
396 the tissue surface. AFM generated Young's moduli of 2.66 kPa for MyoCon, 3.64 kPa for
397 CoCon, and 6.02 kPa for CoTGFβ, with all groups being significantly different from one another
398 (p < 0.01, Fig 5I).

399

400 **Supplementation with TGF-β1 and addition of myofibroblasts enhances myogenesis in**
401 **collagen 1-based hydrogels.**

402 MyoCon, MyoTGFβ, CoCon, and CoTGFβ hydrogels were imaged for myosin heavy chain. In
403 the myoblast control condition lacking TGF-β1 supplementation, some MyHC was present in
404 unfused mononuclear cells, but observable myotube formation was absent (Fig 8A). In contrast,
405 TGF-β1-treated myoblast hydrogels showed robust myotube formation, with somewhat
406 inconsistent alignment orientations (Fig 8B). Without supplementation with TGF-β1, co-cultures
407 with fibroblasts and myoblasts showed small and immature myotube-shaped cells (Fig 8C), in
408 contrast to its TGF-β1-treated counterpart containing myofibroblasts (Fig 8D). CoTGFβ
409 hydrogels yielded the thickest and longest muscle fibers of any condition and possessed the
410 highest degree of multinucleation. These muscle fibers also demonstrated the best alignment.
411 CoTGFβ hydrogels were also more visibly contracted in their culture wells than other conditions
412 (Fig 8E), although MyoTGFβ hydrogels displayed a lesser degree of contraction. Contraction of
413 MyoCon and CoCon hydrogels was not observed.

414

415   **Discussion**

416

417   These experiments investigated the impact of tissue remodeling and ECM deposition on the

418   biomechanical tissue niche; TGF-β1 signaling; and cell-cell signaling between fibroblasts,

419   myofibroblasts, and myoblasts on *in vitro* simulations of myogenesis. Our data demonstrates that

420   transitioning from 2D to 3D culture systems has a profound impact on gene and protein

421   expression involved in mechanotransduction. Consistent with other literature, TGF-β1

422   differentiated fibroblasts to myofibroblasts in 2D cultures containing only fibroblasts (Dahl,

423   Ribeiro, & Lammerding, 2008; Dong et al., 2013; Sandbo & Dulin, 2011), but switching to a 3D

424   culture equivalent resulted in suppression of myofibroblast markers. Additionally, myoblasts

425   have been reported to assume a myofibroblast-like phenotype with TGF-β1 exposure in 2D

426   (Cencetti, Bernacchioni, Nincheri, Donati, & Bruni, 2010; Charge & Rudnicki, 2004; Filvaroff,

427   Ebner, & Derynck, 1994; Li et al., 2004), and our TGF-β1 treated 2D cultures showed similar

428   decreases in myogenecity in monocultures, with the myofibroblast co-culture displaying the most

429   downregulated myogenin expression of any group. *In vivo,* however, while muscle fiber

430   regeneration can be inhibited by exogenous TGF-β1 (Filvaroff et al., 1994; Mendias et al., 2012),

431   endogenous TGF-β1 signaling plays an important role in myogenesis. Genetically truncating the

432   type II TGF-β receptor in myoblasts arrests their ability to differentiate *in vivo*, indicating that

433   TGF-β1 signaling routinely contributes to muscle development and regeneration (Karalaki et al.,

434   2009; Myhre & Pilgrim, 2012). In agreement with these studies, we found that TGF-β1

435   supplementation improved myogenesis in our 3D muscle models, a reversal of the observations

436   in 2D cultures.

437

438   The mechanism for TGF-β1-mediated increases in myogenic differentiation and contractility

439   highlights a differential effect of TGF-β1 on myofibrillogenesis in 2D and 3D systems.

440   Myofibrillogenesis initiates sarcomere development by increasing the dense packing of

441   contractile and cytoskeletal proteins in muscle cells. During myofibrillogenesis, myofibrils are

442   assembled from the framework of the actin cytoskeleton and undergo maturation by successive

443   incorporation of proteins with increasing contractility. This process is driven by transmitting

444   mechanical tension in the actin cytoskeleton to surrounding ECM through costameres (Sanger,

445   Wang, Fan, White, & Sanger, 2010) and results in the development and alignment of sarcomeres

446 (Weist et al., 2013). TGF-β receptor activation increases cytoskeletal polymerization of α-SMA
447 stress fibers in 2D culture platforms (Filvaroff et al., 1994), but also simultaneously has an
448 inhibiting effect on myogenesis. However, since α-SMA is a precursor protein to sarcomeric
449 actin in myofibrillogenesis, moderate TGF-β1 levels in 3D may accelerate myofibrillogenesis
450 through an α-SMA-mediated upregulation mechanism that could increase the tensional forces
451 cells exert on their environment.

452

453 In 3D, fibroblasts and myofibroblasts benefit muscle regeneration through depositing ECM,
454 organizing myoblast differentiation and myotube fusion, and stimulating myofibrillogenesis
455 (Sanger et al., 2010; Turrina et al., 2013). Myotube formation dynamically remodels the
456 biomechanical environment within muscle to further attenuate fibroblast and myofibroblast
457 activity. *In vitro* cell traction studies have shown that myotubes exert 5-8 times greater traction
458 forces on their substrates than fibroblasts, and these forces increase as myotubes mature (Dahl et
459 al., 2008). Contracting myotubes transmit their forces to surrounding ECM through costameres
460 and exert tensional forces throughout the muscle organ to facilitate contraction (Costa, 2014).
461 This mechanism of force transmission could explain the greater recoil and shortening capacity in
462 our co-culture tissues in contrast to myoblast-only samples with a suppressed ability to disperse
463 forces to the surrounding ECM. The relative absence of supportive ECM for myotubes in self-
464 assembled monocultures decreases the availability for integrin connections to the tissue
465 microenvironment and reduces tensional forces applied to surrounding structures, resulting in
466 less elastic recoil after being released from tension. Additionally, our data showing lower elastic
467 moduli in 3D myoblast monocultures than co-cultures is congruent with the findings of Meyer
468 and Lieber, who found the elastic stiffness of skeletal muscle fibers to be significantly dependent
469 on the presence of ECM. In their study, dissected muscle fibers stripped of their extracellular
470 matrix sheaths had four-fold lower elastic moduli than fascicles that retained their ECM (Meyer
471 & Lieber, 2011).

472

473 3D fibroblast and myofibroblast co-cultures were distinct in their morphology, force
474 transmission capacities, and biomechanical properties. The bundling of highly multinucleated
475 myotubes in parallel within CoTGFβ constructs was more similar to *in vivo* muscle fascicle
476 morphology than fibroblast co-cultures, and was accompanied by the greatest upregulation in

477   myogenin expression of all groups. Enhanced muscle fiber maturation and patterning likely
478   increased the magnitude of zero-force shortening in CoTGFβ samples due to acto-myosin
479   kinetics. This is in accordance with a study by Larkin et. al, who found that TGF-β1 treatment of
480   heterogeneous fibroblast and satellite cell populations in engineered muscle constructs increased
481   their force generation capacities during electrical stimulation (Weist et al., 2013). Our study
482   further identifies that the activation of myofibroblasts from fibroblasts benefits myogenesis
483   during co-culturing with myoblasts, due in part to their enhanced ECM generation. The tenacity
484   of myofibroblasts in co-culture is demonstrated through the highest collagen 1 gene expression
485   of all conditions, where collagen 1 reinforcement likely improved tissue integrity and stiffness
486   from TGF-β1 treatment. Additionally, we have shown that TGF-β1 treatment in monocultures of
487   myoblasts also improves muscle differentiation in 3D tissue-engineered cultures.

488

489   **Conclusions**

490

491   The tissue-engineered TGF-β1-treated myoblast and myofibroblast co-culture model is a
492   promising candidate for therapeutic treatment of volumetric muscle loss and can be used as a
493   screening tool for pharmaceutical trials on muscle regeneration. Additionally, this model can be
494   used to improve meat quality of *in vitro* meat, which has experienced accelerated interest in
495   recent years (Langelaana, 2010; Post, 2012). Because of growing awareness of the livestock
496   sector's contribution to worsening climate change, deforestation of the rain forests, reductions in
497   biodiversity, environmental degradation (Steinfeld, 2006), and increased bacterial resistance to
498   antibiotics (Frieden, 2013), devising a sustainable solution for biomanufactured meat production
499   is imperative. *In vitro* meat is a significantly more sustainable solution to traditional factory
500   farming as it uses less food, water, and land resources; produces less greenhouse gases; requires
501   less energy for production (Tuomisto & de Mattos, 2011); and does not require antibiotic misuse.
502   Since meat quality is dependent, in part, on sarcomere development, muscle fiber type, and
503   connective tissue content (Joo, Kim, Hwang, & Ryu, 2013), including TGF-β1 as a cell culture
504   media supplement and co-culturing muscle cells with myofibroblasts can produce meat with
505   flavor and texture increasingly similar to that derived from livestock.

506

507   Although our self-assembled CoTGFβ model of skeletal muscle achieved structural similarity to

508   muscle fascicles, utilizing this self-assembly strategy for scale up of tissue engineering is not

509   practical. Here we have shown that the CoTGFβ technique can be used in hydrogel-based

510   systems, which possess flexibility in design parameters to incorporate vasculature (Koffler et al.,

511   2011; Levenberg et al., 2005). Additionally, electrical stimulation of muscle fibers further

512   matures *in vitro* skeletal muscle models by accelerating sarcomere development (Langelaan et

513   al., 2011) and increasing contraction force (Fuoco et al., 2015; Ito et al., 2014). Accordingly,

514   applying vascularization and electrical stimulation regimens to TGF-β1-treated myofibroblast

515   co-cultures holds promise for skeletal muscle tissue engineering techniques to continue to

516   improve their recapitulation of native muscle.

517

518   **Acknowledgements**

519

520   The authors thank Dr. Marsha Rolle at Worcester Polytechnic Institute for graciously providing a

521   PDMS mold from which agarose molds were based, Dr. William Chillian at Northeast Ohio

522   Medical University for supplying C2C12 cells for experiments, and Dr. Zhenyu Jia at Northeast

523   Ohio Medical University for his assistance with the statistics used in this study.

524

525

526

527

528

529

530

531

532

533

534

535

536
537   **References**

538

539   Cencetti, F., Bernacchioni, C., Nincheri, P., Donati, C., & Bruni, P. (2010). Transforming growth
540   factor-beta1 induces transdifferentiation of myoblasts into myofibroblasts via up-
541   regulation of sphingosine kinase-1/S1P3 axis. *Mol Biol Cell, 21*(6), 1111-1124.
542   doi:10.1091/mbc.E09-09-0812

543   Charge, S. B., & Rudnicki, M. A. (2004). Cellular and molecular regulation of muscle
544   regeneration. *Physiol Rev, 84*(1), 209-238. doi:10.1152/physrev.00019.2003

545   Claflin, D. R., & Faulkner, J. A. (1985). Shortening velocity extrapolated to zero load and
546   unloaded shortening velocity of whole rat skeletal muscle. *J Physiol, 359*, 357-363.

547   Costa, M. L. (2014). Cytoskeleton and Adhesion in Myogenesis. *ISRN Developmental Biology,*
548   *2014*. doi:10.1155/2014/713631

549   Dahl, K. N., Ribeiro, A. J., & Lammerding, J. (2008). Nuclear shape, mechanics, and
550   mechanotransduction. *Circ Res, 102*(11), 1307-1318.
551   doi:10.1161/CIRCRESAHA.108.173989

552   Dong, Y., Lakhia, R., Thomas, S. S., Dong, Y., Wang, X. H., Silva, K. A., & Zhang, L. (2013).
553   Interactions between p-Akt and Smad3 in injured muscles initiate myogenesis or
554   fibrogenesis. *Am J Physiol Endocrinol Metab, 305*(3), E367-375.
555   doi:10.1152/ajpendo.00644.2012

556   Engler, A. J., Sen, S., Sweeney, H. L., & Discher, D. E. (2006). Matrix elasticity directs stem cell
557   lineage specification. *Cell, 126*(4), 677-689. doi:10.1016/j.cell.2006.06.044

558   Filvaroff, E. H., Ebner, R., & Derynck, R. (1994). Inhibition of myogenic differentiation in
559   myoblasts expressing a truncated type II TGF-beta receptor. *Development, 120*(5), 1085-
560   1095.

561   Frieden, T. (2013). *Antibiotic Resistance Threats in the United States*. Retrieved from
562   http://www.cdc.gov/drugresistance/pdf/ar-threats-2013-508.pdf.

563   Fuoco, C., Rizzi, R., Biondo, A., Longa, E., Mascaro, A., Shapira-Schweitzer, K., . . . Gargioli,
564   C. (2015). In vivo generation of a mature and functional artificial skeletal muscle. *EMBO*
565   *Mol Med, 7*(4), 411-422. doi:10.15252/emmm.201404062

566 Gilbert, P. M., Havenstrite, K. L., Magnusson, K. E., Sacco, A., Leonardi, N. A., Kraft, P., . . .
567   Blau, H. M. (2010). Substrate elasticity regulates skeletal muscle stem cell self-renewal
568   in culture. *Science, 329*(5995), 1078-1081. doi:10.1126/science.1191035

569 Godbout, C., Follonier Castella, L., Smith, E. A., Talele, N., Chow, M. L., Garonna, A., & Hinz,
570   B. (2013). The mechanical environment modulates intracellular calcium oscillation
571   activities of myofibroblasts. *PLoS One, 8*(5), e64560. doi:10.1371/journal.pone.0064560

572 Gwyther, T. A., Hu, J. Z., Christakis, A. G., Skorinko, J. K., Shaw, S. M., Billiar, K. L., & Rolle,
573   M. W. (2011). Engineered vascular tissue fabricated from aggregated smooth muscle
574   cells. *Cells Tissues Organs, 194*(1), 13-24. doi:10.1159/000322554

575 Hill, M., Wernig, A., & Goldspink, G. (2003). Muscle satellite (stem) cell activation during local
576   tissue injury and repair. *J Anat, 203*(1), 89-99.

577 Ito, A., Yamamoto, Y., Sato, M., Ikeda, K., Yamamoto, M., Fujita, H., . . . Kamihira, M. (2014).
578   Induction of functional tissue-engineered skeletal muscle constructs by defined electrical
579   stimulation. *Sci Rep, 4*, 4781. doi:10.1038/srep04781

580 Janson, D., Rietveld, M., Willemze, R., & El Ghalbzouri, A. (2013). Effects of serially passaged
581   fibroblasts on dermal and epidermal morphogenesis in human skin equivalents.
582   *Biogerontology, 14*(2), 131-140. doi:10.1007/s10522-013-9416-9

583 Joo, S. T., Kim, G. D., Hwang, Y. H., & Ryu, Y. C. (2013). Control of fresh meat quality
584   through manipulation of muscle fiber characteristics. *Meat Sci, 95*(4), 828-836.
585   doi:10.1016/j.meatsci.2013.04.044

586 Josephson, R. K., & Edman, K. A. (1998). Changes in the maximum speed of shortening of frog
587   muscle fibres early in a tetanic contraction and during relaxation. *J Physiol, 507 (Pt 2)*,
588   511-525.

589 Karalaki, M., Fili, S., Philippou, A., & Koutsilieris, M. (2009). Muscle regeneration: cellular and
590   molecular events. *In Vivo, 23*(5), 779-796.

591 Koffler, J., Kaufman-Francis, K., Shandalov, Y., Egozi, D., Pavlov, D. A., Landesberg, A., &
592   Levenberg, S. (2011). Improved vascular organization enhances functional integration of
593   engineered skeletal muscle grafts. *Proc Natl Acad Sci U S A, 108*(36), 14789-14794.
594   doi:10.1073/pnas.1017825108

595 Langelaan, M. L., Boonen, K. J., Rosaria-Chak, K. Y., van der Schaft, D. W., Post, M. J., &
596   Baaijens, F. P. (2011). Advanced maturation by electrical stimulation: Differences in

597   response between C2C12 and primary muscle progenitor cells. *J Tissue Eng Regen Med,*

598   *5*(7), 529-539. doi:10.1002/term.345

599   Langelaana, M. B., K.; Polak, R.; Baaijens, F.; Post, M.; van der Schaft, D. (2010). Meet the new

600   meat: tissue engineered skeletal muscle. *Trends in Food Science and Technology, 21*(2),

601   59-66. doi:10.1016/j.tifs.2009.11.001

602   Le Grand, F., & Rudnicki, M. A. (2007). Skeletal muscle satellite cells and adult myogenesis.

603   *Curr Opin Cell Biol, 19*(6), 628-633. doi:10.1016/j.ceb.2007.09.012

604   Levenberg, S., Rouwkema, J., Macdonald, M., Garfein, E. S., Kohane, D. S., Darland, D. C., . . .

605   Langer, R. (2005). Engineering vascularized skeletal muscle tissue. *Nat Biotechnol,*

606   *23*(7), 879-884. doi:10.1038/nbt1109

607   Li, Y., Foster, W., Deasy, B. M., Chan, Y., Prisk, V., Tang, Y., . . . Huard, J. (2004).

608   Transforming growth factor-beta1 induces the differentiation of myogenic cells into

609   fibrotic cells in injured skeletal muscle: a key event in muscle fibrogenesis. *Am J Pathol,*

610   *164*(3), 1007-1019.

611   Lieber, R. L., & Ward, S. R. (2013). Cellular mechanisms of tissue fibrosis. 4. Structural and

612   functional consequences of skeletal muscle fibrosis. *Am J Physiol Cell Physiol, 305*(3),

613   C241-252. doi:10.1152/ajpcell.00173.2013

614   Mann, C. J., Perdiguero, E., Kharraz, Y., Aguilar, S., Pessina, P., Serrano, A. L., & Munoz-

615   Canoves, P. (2011). Aberrant repair and fibrosis development in skeletal muscle. *Skelet*

616   *Muscle, 1*(1), 21. doi:10.1186/2044-5040-1-21

617   Mendias, C. L., Gumucio, J. P., Davis, M. E., Bromley, C. W., Davis, C. S., & Brooks, S. V.

618   (2012). Transforming growth factor-beta induces skeletal muscle atrophy and fibrosis

619   through the induction of atrogin-1 and scleraxis. *Muscle Nerve, 45*(1), 55-59.

620   doi:10.1002/mus.22232

621   Meyer, G. A., & Lieber, R. L. (2011). Elucidation of extracellular matrix mechanics from muscle

622   fibers and fiber bundles. *J Biomech, 44*(4), 771-773. doi:10.1016/j.jbiomech.2010.10.044

623   Murphy, M. M., Lawson, J. A., Mathew, S. J., Hutcheson, D. A., & Kardon, G. (2011). Satellite

624   cells, connective tissue fibroblasts and their interactions are crucial for muscle

625   regeneration. *Development, 138*(17), 3625-3637. doi:10.1242/dev.064162

626 Myhre, J. L., & Pilgrim, D. B. (2012). At the Start of the Sarcomere: A Previously Unrecognized
627   Role for Myosin Chaperones and Associated Proteins during Early Myofibrillogenesis.
628   *Biochem Res Int, 2012*, 712315. doi:10.1155/2012/712315
629 Post, M. J. (2012). Cultured meat from stem cells: challenges and prospects. *Meat Sci, 92*(3),
630   297-301. doi:10.1016/j.meatsci.2012.04.008
631 Reggiani, C. (2007). When fibres go slack and cross bridges are free to run: a brilliant method to
632   study kinetic properties of acto-myosin interaction. *J Physiol, 583*(Pt 1), 5-7.
633   doi:10.1113/jphysiol.2007.137000
634 Sandbo, N., & Dulin, N. (2011). Actin cytoskeleton in myofibroblast differentiation:
635   ultrastructure defining form and driving function. *Transl Res, 158*(4), 181-196.
636   doi:10.1016/j.trsl.2011.05.004
637 Sanes, J. R. (2003). The basement membrane/basal lamina of skeletal muscle. *J Biol Chem,*
638   *278*(15), 12601-12604. doi:10.1074/jbc.R200027200
639 Sanger, J. W., Wang, J., Fan, Y., White, J., & Sanger, J. M. (2010). Assembly and dynamics of
640   myofibrils. *J Biomed Biotechnol, 2010*, 858606. doi:10.1155/2010/858606
641 Smith, L. R., Lee, K. S., Ward, S. R., Chambers, H. G., & Lieber, R. L. (2011). Hamstring
642   contractures in children with spastic cerebral palsy result from a stiffer extracellular
643   matrix and increased in vivo sarcomere length. *J Physiol, 589*(Pt 10), 2625-2639.
644   doi:10.1113/jphysiol.2010.203364
645 Steinfeld, H. G., P.; Wassenaar, T.; Castel, V.; Rosales, M.; de Haan, C. (2006). *Livestock's Long*
646   *Shadow: Environmental Issues and Options*. Rome : Food and Agriculture Organization
647   of the United Nations.
648 Tuomisto, H. L., & de Mattos, M. J. (2011). Environmental impacts of cultured meat production.
649   *Environ Sci Technol, 45*(14), 6117-6123. doi:10.1021/es200130u
650 Turrina, A., Martinez-Gonzalez, M. A., & Stecco, C. (2013). The muscular force transmission
651   system: role of the intramuscular connective tissue. *J Bodyw Mov Ther, 17*(1), 95-102.
652   doi:10.1016/j.jbmt.2012.06.001
653 Weist, M. R., Wellington, M. S., Bermudez, J. E., Kostrominova, T. Y., Mendias, C. L., Arruda,
654   E. M., & Larkin, L. M. (2013). TGF-beta1 enhances contractility in engineered skeletal
655   muscle. *J Tissue Eng Regen Med, 7*(7), 562-571. doi:10.1002/term.551
656

Technical protocol for 2D/3D culture systems and experimental conditions design

(Upper) *Technique*: 2D cell culture and 3D tissue engineering protocols involve an initial high serum culture period on standard cell culture plates to separately amplify myoblast and fibroblast populations, with a subset of 'preconditioned' fibroblasts being treated with TGF-β1 to differentiate them into myofibroblasts. After 6 days the cells are passaged and either replated on cell culture plates for 2D studies or used for 3D systems. Our 3D systems included a scaffoldless self-assembly method for tissue engineering and a collagen 1 hydrogel based-technique. A low serum culture period subsequently follows, lasting 7 days, and some groups are supplemented with TGF-β1. The black arrow denotes the location of a tissue construct around the annulus inside an agarose mold, scale bar = 2mm. (Lower) *Conditions*: Experimental design is defined by comparisons between culture systems (2D culture plates vs 3D agarose gels/collagen 1-based hydrogels), cellular content (co-culture or monoculture of myoblasts, fibroblasts, or myofibroblasts), and their biochemical treatment in culture (±TGF-β1). The resulting group identification terms code for the conditions investigated in these experiments.

Cell Amplification /
± Preconditioning

Cell Culture

2D CULTURES

Tissue Self-Assembly

3D CULTURES

Collagen 1-Based Hydrogels

6D, ↑ SERUM ± TGFβ   **PASSAGE**   **7D, ↓ SERUM ± TGFβ**
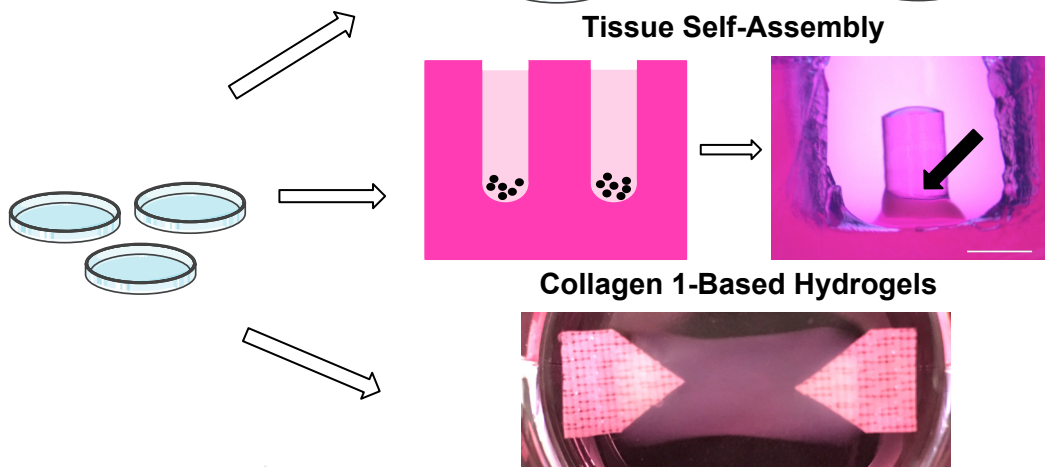
	Cells	Treatment	Group ID
2D	Fibroblast/ Myofibroblast/ Myoblast monocultures	Untreated control	2D FibCon / 2D MyoCon
		+TGF-β	2D FibTGFβ / 2D MyoTGFβ
	Co-culture	Untreated control	2D CoCon
		+TGF-β	2D CoTGFβ
3D	Fibroblast/ Myofibroblast/ Myoblast monocultures	Untreated control	3D FibCon / 3D MyoCon
		+TGF-β	3D FibTGFβ / 3D MyoTGFβ
	Co-culture	Untreated control	3D CoCon
		+TGF-β	3D CoTGFβ

Immunostaining and morphological characterization of 2D cultures

2D FibCon (A) and FibTGFβ (B) stained for α-SMA and DAPI, and FibCon (C) and FibTGFβ (D) stained for procollagen. 2D MyoCon (E), MyoTGFβ (F), CoCon (G), and CoTGFβ (H) conditions stained for myosin heavy chain (MyHC) and DAPI. Scale bars = 100μm for all images. Quantitative analysis of average area of procollagen signal/average number of nuclei per field of view (I), nuclei circularity (J), and average number of total nuclei per field of view (K) in FibCon and FibTGFβ samples. Quantitative analysis of myotube alignment (L) in MyoCon and CoCon cultures, reported as the standard deviation of myotube alignment angles. Graphs display group averages with standard error bars.
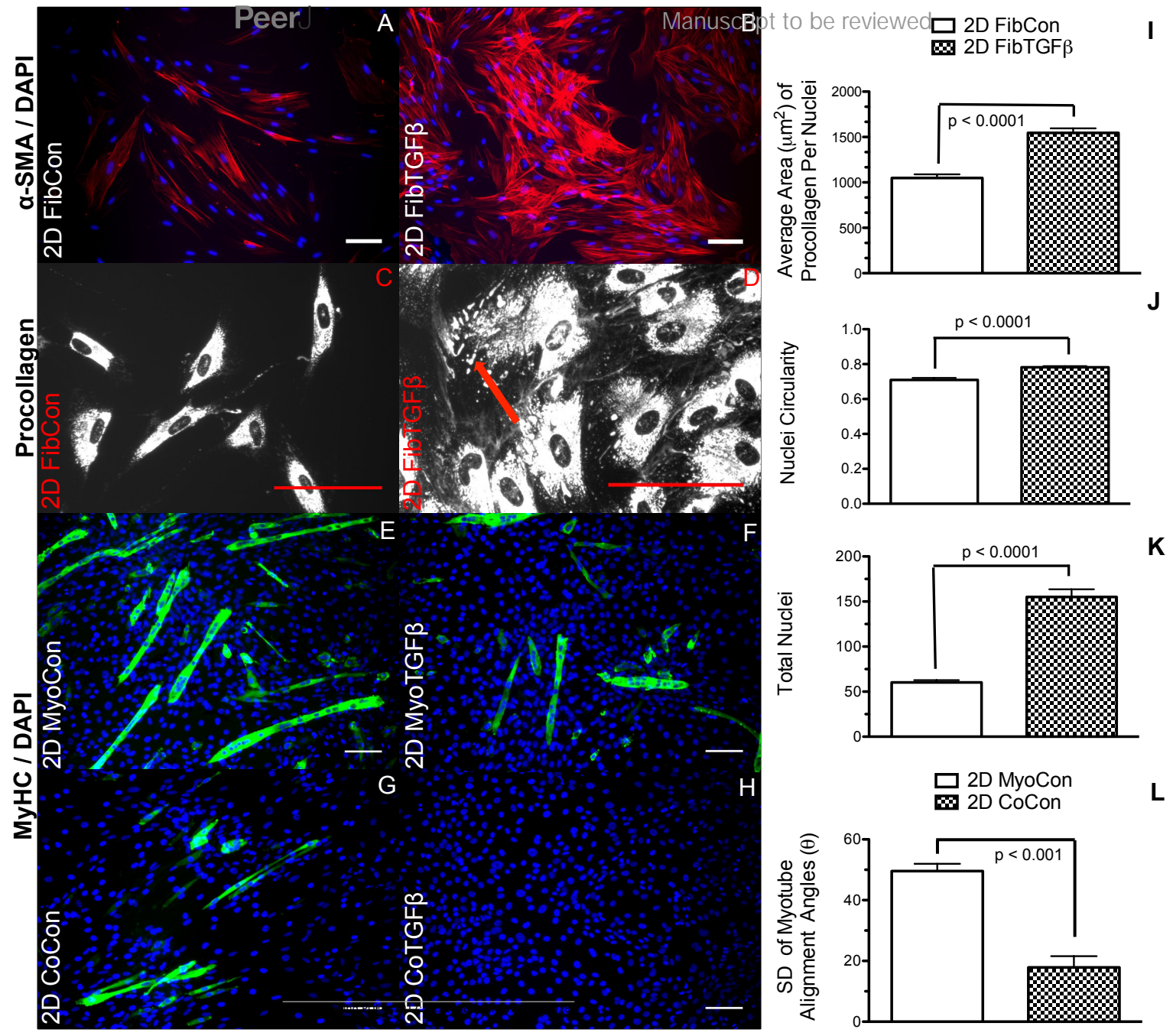
Gene expression of fibroblast collagen 1 and α-SMA and myoblast myogenin in 2D cell cultures and 3D self-assembled tissue conditions

Species-specific gene expression for all groups is normalized to gene expression for group (a), 2D FibCon or MyoCon samples. Average fold change values are reported with standard error bars. Significance values were defined at $p < 0.01$. (A) α-SMA: (a) is significantly different from (b), (d), (e), (f), (g), and (h); (b) is significantly different from (c), (e), (f), (g), and (h); (c) is significantly different from (e), (f), (g), and (h); (d) is significantly different from (e), (f), (g), and (h); (e) is significantly different from (g) and (h); and (f) is significantly different from (g) and (h). (B) COL1: (a) is significantly different from (e), (f), and (h); (b) is significantly different from (c), (e), (f), and (h); (c) is significantly different from (e), (f), and (h); (d) is significantly different from (e), (f), and (h); (e) is significantly different from (g) and (h); (f) is significantly different from (g) and (h); and (g) is significantly different from (h). (C) MYOG: (a) is significantly different from (b), (c), (d), (e), (g), and (h); (b) is significantly different from (d), (f), (g), and (h); (c) is significantly different from (d), (f), and (h); (d) is significantly different from (e), (f), (g), and (h); (e) is significantly different from (f) and (h); (f) is significantly different from (g) and (h); and (g) is significantly different from (h).
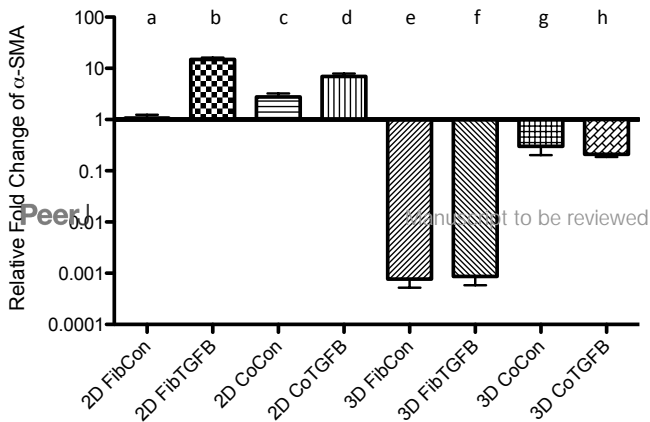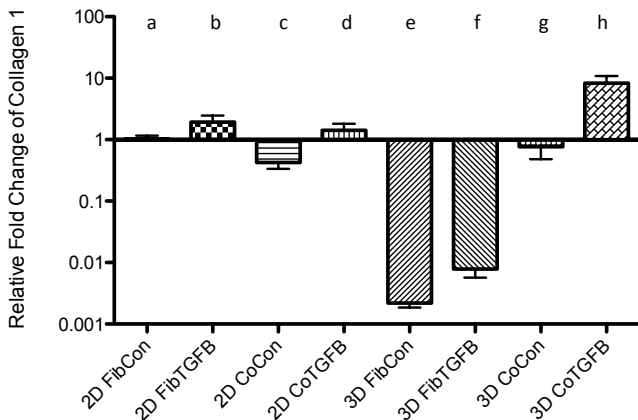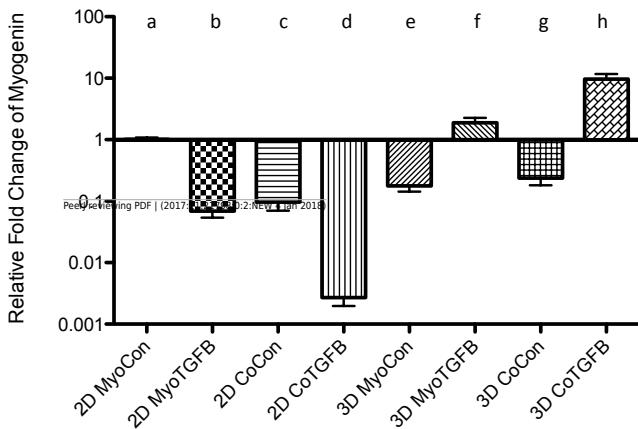
Zero force shortening of self-assembled tissues and their surface characteristics

Tissue shortening was assessed when removed from agarose molds after 3 minutes, 27 minutes, and 24 hours. 3D FibCon (A-C), FibTGFβ (D-F), MyoCon (G-I), MyoTGFβ (J-L), CoCon (M-O), and CoTGFβ tissue rings (P-R), with scale bars = 1000μm. The filled arrow in (D) indicates a structural rupture in the tissue, and the black arrow in (M) indicates thinned myoblast-free region of sample. Higher magnification images of FibCon (S), MyoTGFβ (T), and CoTGFβ tissues (U) show surface texture. In (T), the filled arrow is a large nodule on a MyoTGFβ sample, and unfilled arrows indicate smaller syncytium, scale bars = 300μm.
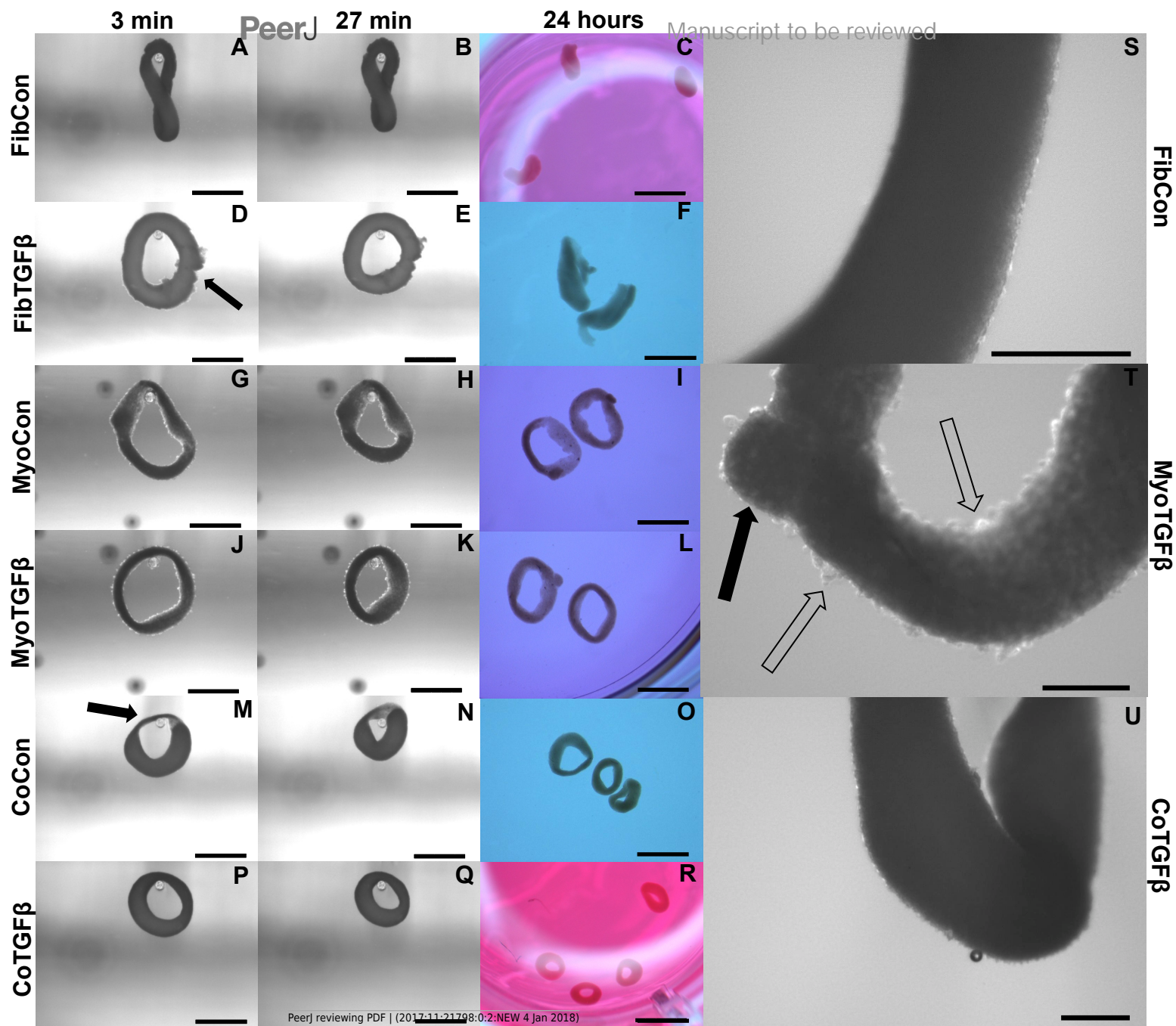
Biomechanical properties of self-assembled tissue constructs

(A) An agarose gel mold with central post and tissue of tissue skewered onto a microbeam from the Microsquisher system. The white arrow denotes the longest axis of the tissue used to track shortening from initial length. C_1 = inner circumferential area and C_2 = outer circumferential area used to measure shrinkage by tissue area, scale bar = 1000µm. (B) Percent (%) of initial length of the longest axis of tissue samples 27 minutes after their removal from agarose gels. All groups shortened from their original size significantly ($p < 0.001$), and the magnitude of change was significantly different between each group ($p < 0.05$), except for (a) and (b). (C) Tissue shortening rate of samples over time. (D) Image of the Microsquisher system used to obtain young's modulus of tissue sections (white asterisk), scale bar = 600µm. (E) The % area of (C_1) / (C_2) in CoCon and CoTGFβ tissues after 24 hours of contraction. (F) Initial thickness of tissue samples, asterisks indicate $p < 0.001$. (G) Screenshot of AFM cantilever and sample (white asterisk), scale bar = 100µm. (H) Young's modulus of tissues generated from Microsquisher force-displacement data. (a) is significantly softer than (e) and (f); (b) is significantly softer than (c), (d), (e), and (f); and (c) and (d) are significantly softer than (f), with $p < 0.001$. (I) Young's modulus of MyoCon, CoCon, and CoTGFβ tissues calculated by AFM, asterisks indicate $p < 0.01$. Graphs display group averages with standard error bars.
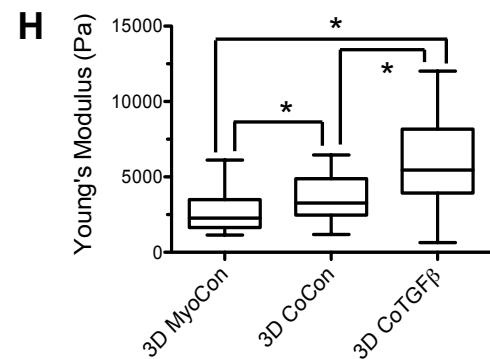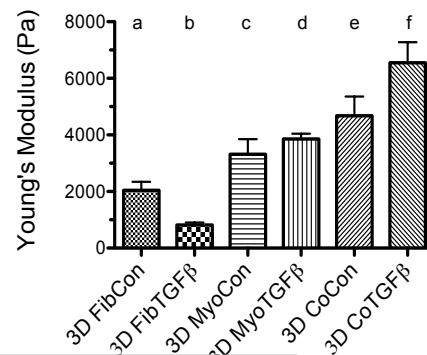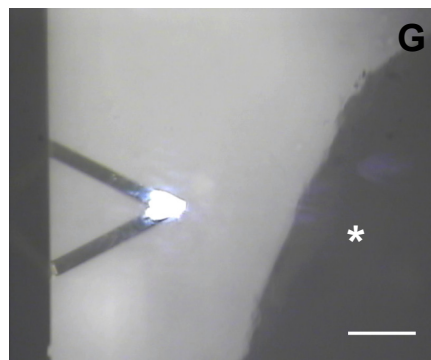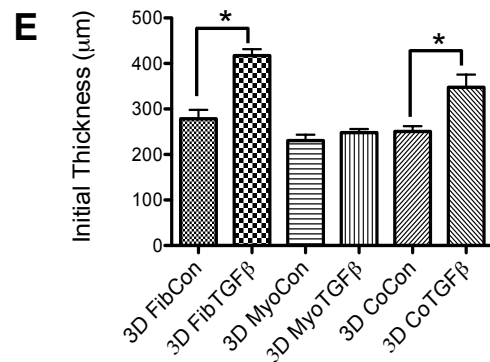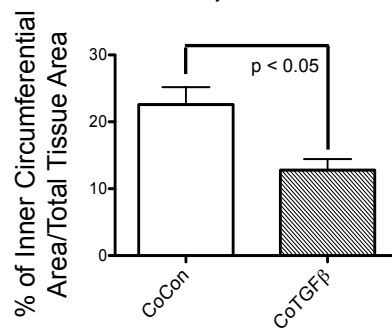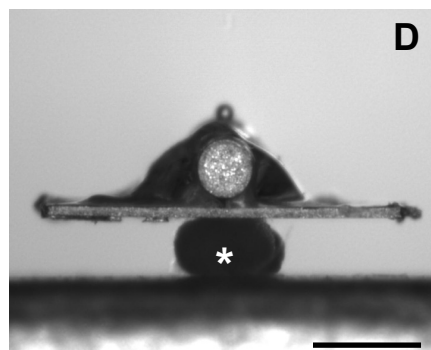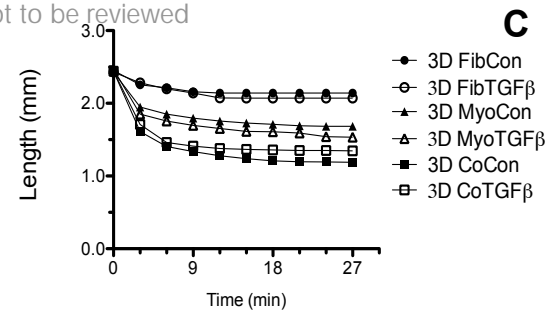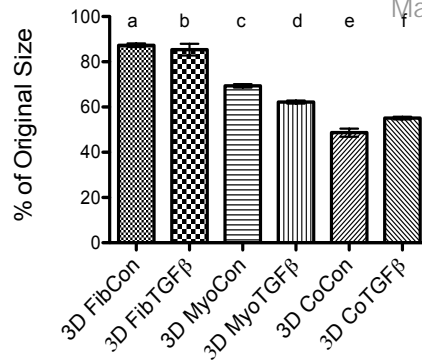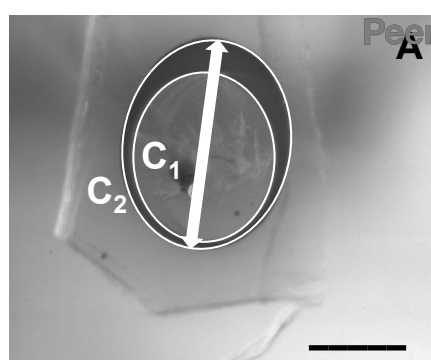
Histology of self-assembled myoblast monocultures

3D MyoCon (A-D, I-K) and MyoTGFβ constructs (E-H) are displayed with myosin heavy chain (A, E, I), MyHC merged with DAPI (B, F, K), and DAPI alone (J). α-SMA (C, G) and α-SMA merged with DAPI (D, H). White filled arrows indicate direction of alignment and anisotropy of myotubes (E), while unfilled arrows indicate unanchored syncytium (A, I), and white asterisks identify regions of tissue breakage (C, G), scale bars = 100μm.
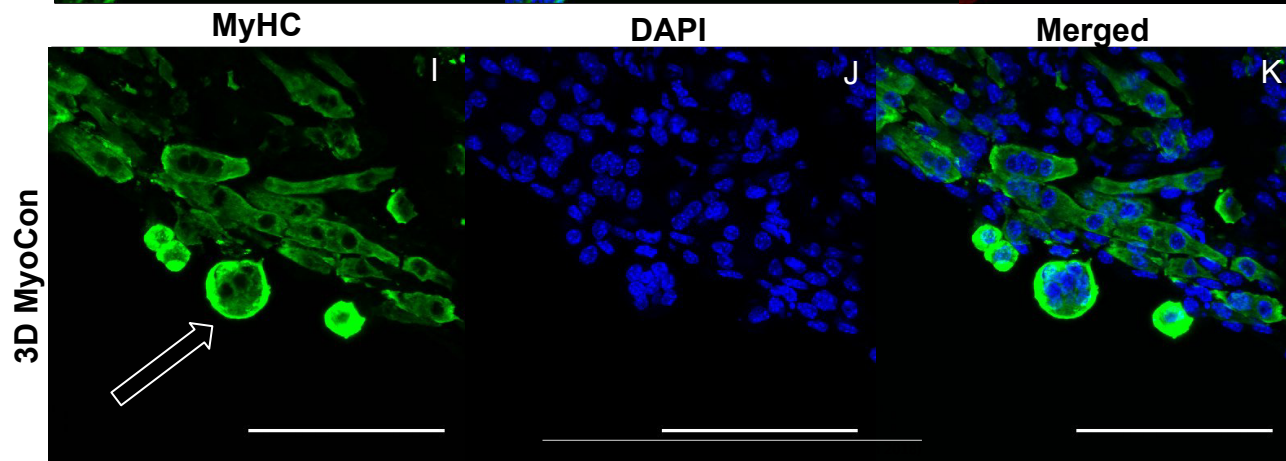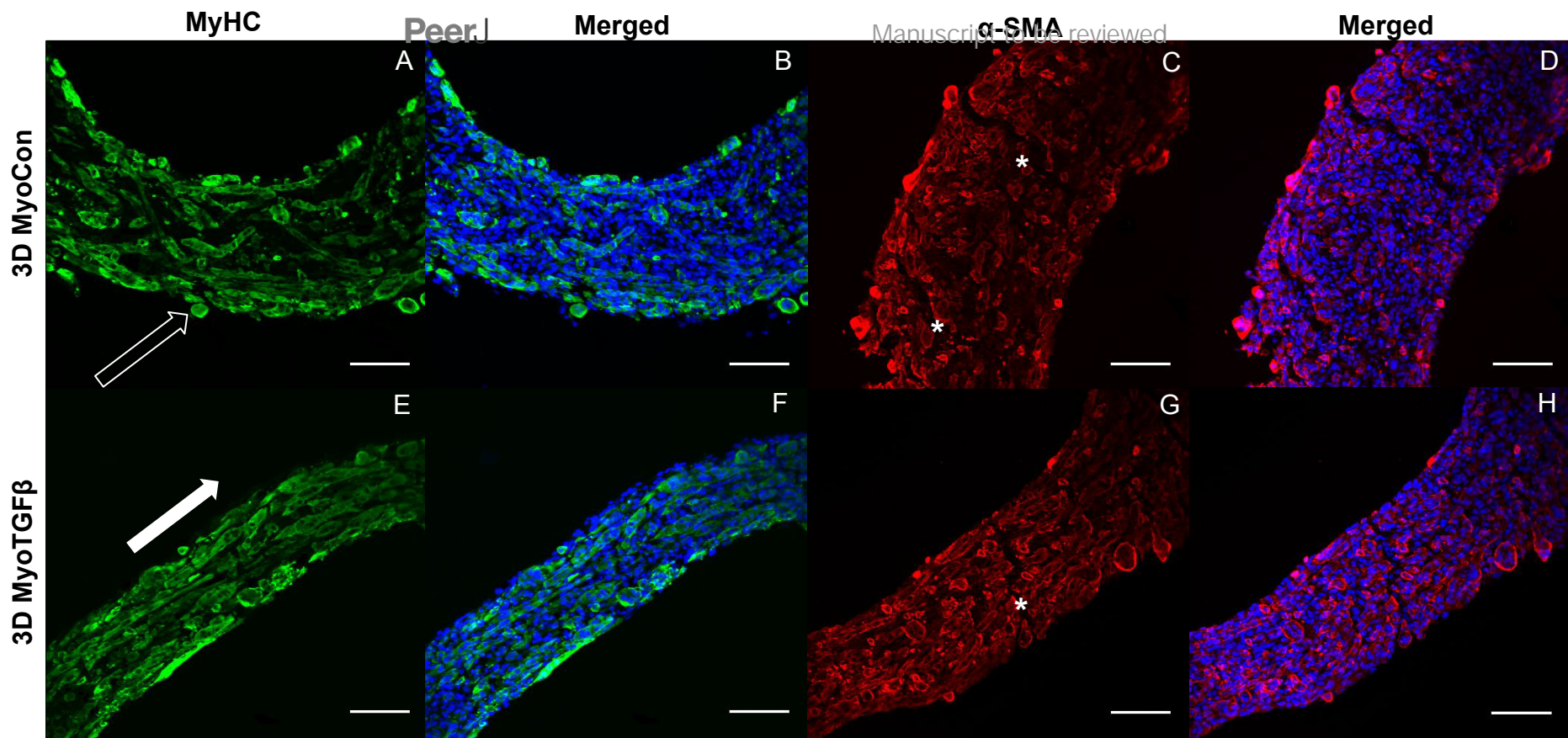
Histology of self-assembled co-cultures

3D CoCon (A, B, E, F, H, I) and CoTGFβ tissues (C, D, G, J, K). α-SMA (A, C) and α-SMA merged with DAPI (B, D). Myosin heavy chain staining of CoCon constructs (E, H), f-actin staining of E (F), and DAPI staining of H (I). MyHC staining of CoTGFβ tissues (G, J, K) with DAPI and f-actin staining (J, K). (J) is an inset of G. White fill arrows indicate cross sections of myotubes observed with MyHC and actin staining, while unfilled arrows show elongated myotubes fused along circumferential axis of tissue rings, scale bar = 100μm.
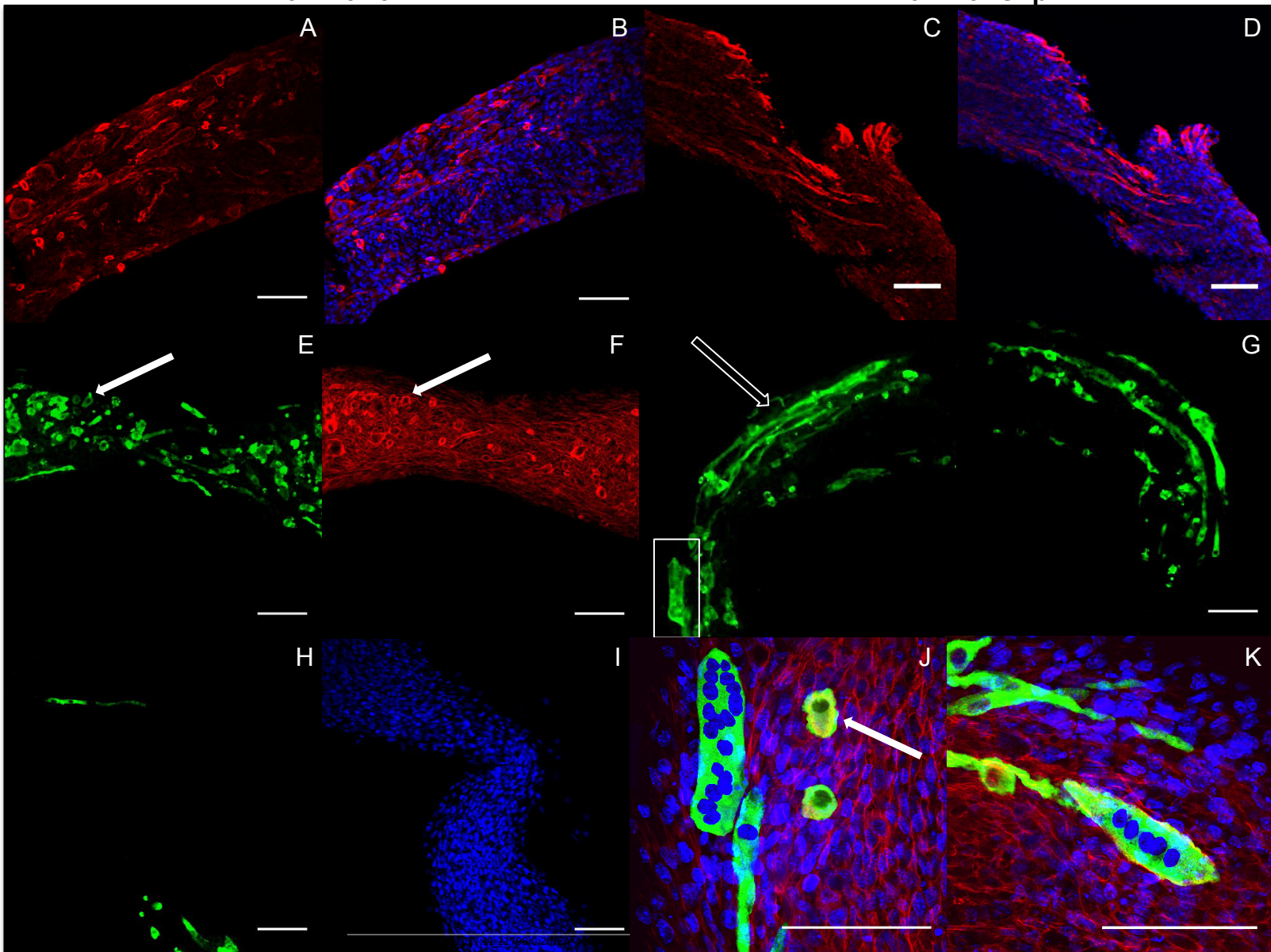
Histology of mono- and co-cultures in collagen 1-based hydrogels

Myosin heavy chain staining of MyoCon (A), MyoTGFβ (B), CoCon (C), and CoTGFβ (D) hydrogels. Scale bar = 100μm. (E) are images of the hydrogels from culture wells of a 6-well plate, in descending order: MyoCon, MyoTGFβ, CoCon, and CoTGFβ hydrogels.

MyoCon

MyoTGFβ

CoCon

CoTGFβ